ACS OMEGA

Article

Cite This: ACS Omega 2019, 4, 5147−5154

http://pubs.acs.org/journal/acsodf

Temperature-Controlled Locally Excited and Twisted Intramolecular Charge-Transfer State-Dependent Fluorescence Switching in Triphenylamine−Benzothiazole Derivatives

Anu Kundu,[†] Subramanian Karthikeyan,[‡] Yoshimitsu Sagara,[§] Dohyun Moon,*[,∥] and Savarimuthu Philip Anthony*[,†]

[†]School of Chemical & Biotechnology, SASTRA Deemed University, Thanjavur 613401, Tamil Nadu, India

[‡]PG and Research Department of Chemistry, Khadir Mohideen College, Adirampattinam, Tamil Nadu 614701, India

[§]Research Institute for Electronic Science, Hokkaido University, N20, W10, Kita-Ku, Sapporo 001-0020, Japan

[∥]Beamline Department, Pohang Accelerator Laboratory, 80 Jigokro-127-beongil, Nam-gu, Pohang, Gyeongbuk, Korea

Supporting Information

ABSTRACT: Triphenylamine−benzothiazole derivatives, *N*-(4-(benzo[*d*]thiazol-2-yl)phenyl)-*N*-phenylbenzenamine (**1**), *N*-(4-(benzo[*d*]thiazol-2-yl)-3-methoxyphenyl)-*N*-phenylbenzenamine (**2**), and 2-(benzo[*d*]thiazol-2-yl)-5-(diphenylamino)-phenol (**3**), showed unusual temperature-controlled locally excited (LE) and twisted intramolecular charge-transfer (TICT) state fluorescence switching in polar solvents. The detailed photophysical studies (absorption, fluorescence, lifetime, and quantum yield) in various solvents confirmed polarity-dependent LE and TICT state formation and fluorescence tuning. **1** and **2** exhibited strong fluorescence with short lifetime in nonpolar solvents compared to polar solvents. **1**, **2**, and **3** in dimethylformamide (DMF) at room temperature showed low-energy weak TICT state fluorescence, whereas high-energy strong LE state fluorescence was observed at −196 °C. Interestingly, further increasing the temperature from 20 to 100 °C, the DMF solution of **1** and **2** exhibited rare fluorescence enhancement with a slight blue shift of λ_{max} via activating more vibrational bands of the TICT state. Thus, **1** and **2** showed weak TICT state fluorescence at room temperature, strong LE state fluorescence at −196 °C, and activation of TICT state at 100 °C. Moreover, molecular conformation and aggregation in the solid state influenced strongly on the fluorescence properties of **1**, **2**, and **3**. Solid-state fluorescence and pH-responsive imidazole nitrogen have been exploited for demonstrating halochromism-induced fluorescence switching. Computational studies provided further insights into the fluorescence tuning and switching. The present studies provide understanding and opportunity to make use of D−A organic molecules in the LE and TICT states for achieving fluorescence switching and tuning.

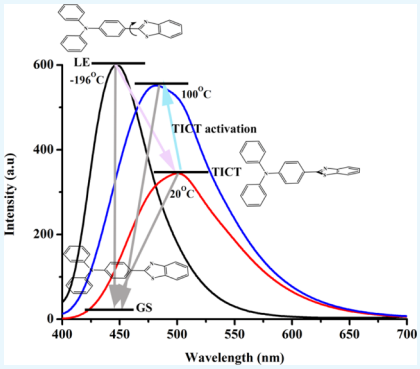

1. INTRODUCTION

Fluorescence switching and tuning of organic molecules received significant attention over the years because of their fundamental importance and application potentials in modern optical and optoelectronic devices.[1−4] Fluorescence phenomena that involve electron transfer, energy transfer, excimer formation, and J or H aggregation have been strongly influenced by fluorophore orientation, conformation, and flexibility. The nonplanar molecular conformation of triphenylamine (TPA) and tetraphenyl ethylene core has been used to generate aggregation-enhanced emissive (AEE) and stimuli-responsive fluorescent materials.[5−7] Conformational flexibility of fluorophores produced polymorphism-induced fluorescence switching and tuning.[8−10] Donor−acceptor (D−A) organic molecules display locally excited (LE) and twisted intramolecular charge-transfer (TICT) state fluorescence depending on the solvent polarity and viscosity that drastically modulated the fluorescence λ_{max} and efficiency.[11,12] Interestingly, the LE and TICT character of D−A molecules can easily be controlled using several factors including steric substituents, conformation, D−A strength, and polarity environments that make the D−A fluorophores highly attractive toward various applications.[13−15] Boron−dipyrromethene-based compounds exhibited transition from nonpolarized fluorescent LE state to nonfluorescent highly polarized TICT state depending on the solvent polarity, which has been used as an environmental polarity sensor.[16,17] Steric restrictions in D−A molecules enabled precise control of the proportion of the LE and TICT state and are used for developing solvatochromic probes and AEE materials.[18−20]

Particularly, TICT-active fluorophores with weak supramolecular interacting functionality that rigidifies the fluoro-

Received: November 6, 2018
Accepted: February 28, 2019
Published: March 12, 2019

DOI: 10.1021/acsomega.8b03099
ACS Omega 2019, 4, 5147−5154

phores and restricts the intramolecular motions are ideal molecules for generating AEE materials with exciting fluorescence properties.[21−23] D−A molecules with hybridized LE- and TICT-based charge-transfer (CT) state were recently proposed for developing efficient electroluminescent and organic light-emitting diode materials.[24−26] The enhancement of TICT-active fluorophore by hampering LE−TICT interconversion in viscous media has been utilized to study the peptide−protein interaction and imaging intracellular microviscosity.[27,28] Although rarely reported, some of the TICT-active fluorophores showed enhancement of fluorescence with increasing temperature via activating more vibrational bands.[29−32] Alkyl-substituted organoboronium bisdiketone showed dramatic fluorescence thermochromism.[33] A ratiometric fluorescence thermometer with a positive temperature coefficient has been demonstrated using *N*,*N*-dimethyl-4-((2-methylquinolin-6-yl)ethynyl)aniline, a TICT-active molecule.[32] Thus, the LE and TICT character of D−A molecules have been exploited to tune the fluorescence and to increase the external quantum efficiency for organic light-emitting diodes. However, utilization of the LE and TICT character of D−A molecules for fluorescence switching in solution by controlling the temperature has been scarcely reported.

TPA, a nonplanar propeller-shaped molecule, has been used as the core unit to generate several AEE and stimuli-responsive smart fluorescent materials including rewritable and self-erasable fluorescent materials.[34−37] Benzothiazole, a heterocyclic aromatic ring with electron-deficient sulfur atom, has often been employed to improve the D−A character and fluorescence intensity of organic molecules.[38,39] The integrating benzothiazole with TPA produced electroluminescent, solvatochromic, and fluorescence sensing molecules.[40−44] Benzothiazole has also extensively explored for generating solid-state fluorescent materials based on excited-state intramolecular proton-transfer mechanism.[45] We are interested in developing smart fluorescent materials that respond to various external stimuli including temperature, pressure, solvent, and pH.[46,47] Hence, we envisage that integrating mechanochromic TPA with pH-responsive benzothiazole might produce multi-stimuli-responsive fluorescent materials, especially halochromism-induced rewritable and self-erasable fluorescent platforms. In this manuscript, we report the synthesis of TPA−benzothiazole derivatives, *N*-(4-(benzo[*d*]thiazol-2-yl)-phenyl)-*N*-phenylbenzenamine (**1**), *N*-(4-(benzo[*d*]thiazol-2-yl)-3-methoxyphenyl)-*N*-phenylbenzenamine (**2**), and 2-(benzo[*d*]thiazol-2-yl)-5-(diphenylamino)phenol (**3**), and unusual temperature-controlled LE and TICT state fluorescence switching in dimethylformamide (DMF). Absorption and fluorescence spectra of all three compounds revealed solvent polarity-dependent LE and TICT character. **1** and **2** exhibited strong fluorescence in nonpolar solvents compared to polar solvents. **3** exhibited relatively weak fluorescence in solution because of a labile phenolic hydroxyl functional group. **1**, **2**, and **3** showed TICT, LE, and rare TICT-activated state emission in DMF depending on the temperature. Solid-state structural studies were performed to establish the role of molecular conformation and organization on solid-state fluorescence.

2. RESULTS AND DISCUSSION

1, **2**, and **3** molecules (Scheme 1) were synthesized from the corresponding aldehyde as described in Scheme S1.[41,42] The absorption spectra of **1**, **2**, and **3** in various solvents did not show significant modulation of peak position. The intramolecular CT band between electron-rich TPA and electron-deficient benzothiazole appeared between 370 and 374 nm for **1**, whereas **2** revealed absorption between 372 and 378 nm (Figure S7a,b). **3** showed λ_{max} between 381 and 391 nm in different solvents (Figure S7c). The slight red shift of absorption peak in **2** and **3** could be attributed to methoxy and hydroxyl donor groups. The similar absorption wavelength at different solvent polarity indicates that all compounds showed only slight change of dipole in the ground state. In contrast, the fluorescence spectra of **1**, **2**, and **3** exhibited typical solvent polarity-dependent bathochromism. **1** showed a fluorescence shift from 434 nm in toluene to 501 nm in CH_3CN (Figure 1a). The fluorescence of **2** and **3** red-shifted from 422 nm in toluene to 480 nm in CH_3CN and 438 in toluene to 503 nm in CH_3CN, respectively (Figures 1b and S8). This indicates that the excited states of the molecules might be significantly polar to be affected by the solvent polarity. The excited-state dipole moments (μ_e) of **1** and **2** were calculated from the slope of the Stokes shift ($\nu_a-\nu_f$) using the Lippert-Mataga equation, which was drawn against the orientation of polarizability (f). The plot of Stokes shift against solvent polarizability shows clearly two linear regions that indicate two distinct excited states for low and high polarity (Figure 1c,d). The calculated ground state is 3.37 and 6.33 D, respectively. Accordingly, the excited-state dipole (μ_e) values in toluene and DMF are calculated to be 8.8 and 12.42 D (**1**) and 10.28 and 13.38 D (**2**) that could be attributed to the LE and TICT state, respectively.[49,50] The slight absorption λ_{max} changes and large bathochromic fluorescence in different solvent polarity suggest the formation of TICT state in polar solvents.[11,32] In nonpolar solvents, the dipole (μ_g) of **1** and **2** in toluene is 2.94 and 5.58 D and DMF shows stronger quantum yield (Φ_f) compared to polar solvents (Table 1). The strong fluorescence with blue-shifted emission in nonpolar solvents is attributed to high-energy LE state, whereas comparatively weak and red-shifted emission from polar solvent is attributed to TICT state (Scheme 2). In nonpolar solvents, the D−A fluorophore adopts coplanar conformation, which was stabilized via the mesomeric interaction between the π-orbitals of D and A units. In contrast, D−A fluorophores undergo fast intramolecular CT accompanied by an intramolecular D−A-twisted structure around the single bond in polar solvents and produces a relaxed perpendicular structure (Scheme 2).[11] The nonradiative relaxation of D−A from TICT state often leads to weak or nonfluorescence in polar solvents. The excited-state lifetime measurements of **1** and **2** across different solvent polarity revealed single exponential decay with the increase of lifetime with solvent polarity (Table 2, Figure S9). This also further supports the formation of TICT state in polar solvents.[11,51] **3** fluorophore showed weak fluorescence in all solvents, which might be due to the presence of acidic hydroxyl functionality.

Scheme 1. Molecular Structure of TPA−Benzothiazole Derivatives

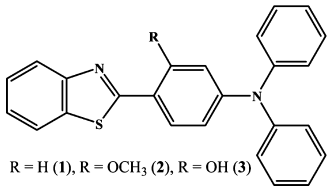

R = H (**1**), R = OCH_3 (**2**), R = OH (**3**)

DOI: 10.1021/acsomega.8b03099
ACS Omega 2019, 4, 5147−5154

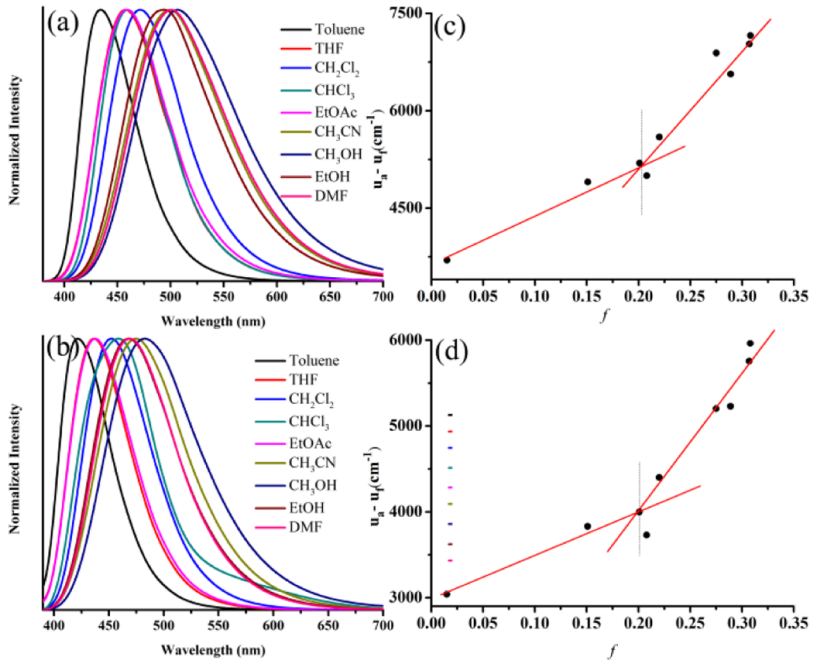

Figure 1. Fluorescence spectra of (a) **1** and (b) **2** in different solvents (10^{-5} M). Linear correlation of the orientation polarization (f) of the solvent with Stokes shift ($\nu_a - \nu_f$) for (c) **1** and (d) **2**.

Table 1. Quantum Yield of 1, 2, and 3

	quantum yield (Φ_f) (compared to 9,10-diphenylanthracene)					
	toluene	CH_2Cl_2	EtOAc	CH_3CN	CH_3OH	DMF
1	0.87	0.79	0.69	0.44	0.28	0.26
2	0.91	0.80	0.72	0.49	0.37	0.60
3	0.12	0.17	0.09	0.15	0.05	0.16

Scheme 2. Jablonski Diagram of LE and TICT Dynamics; GS = Ground State

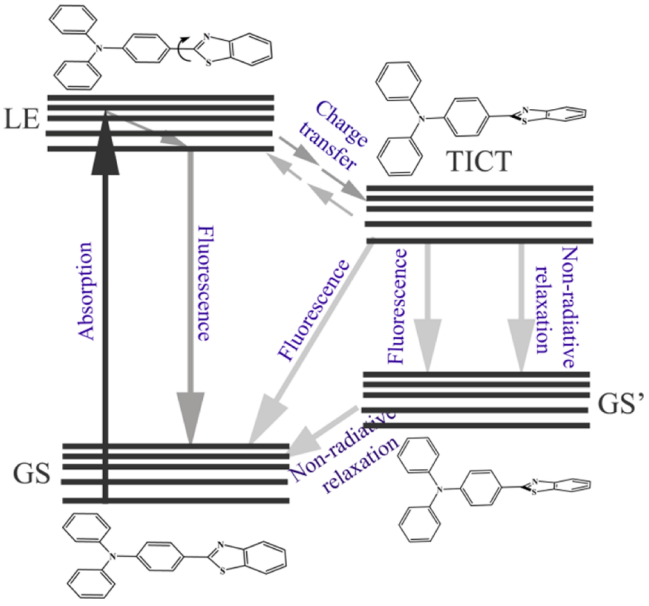

1 showed LE state fluorescence at 432 nm in toluene, whereas low-energy TICT state fluorescence at 501 nm in DMF solution (Figure 1a). **2**, **3** showed fluorescence at 422 and 438 nm in toluene and 470 and 467 nm in DMF, respectively. CH_3CN, CH_3OH, and ethanol solutions of **1** and **2** also showed fluorescence λ_{max} similar to DMF. Interestingly, all three compounds exhibited strong blue-shifted emission with drastic enhancement of intensity upon cooling DMF solution at −196 °C (Figures 2, S10, and S11). The fluorescence of **1** was blue-shifted from 501 to 447 nm with 2 times enhancement of intensity compared to room temperature. Fifteen and three times enhancement of fluorescence intensity was observed for **2** and **3**, respectively, compared to room temperature. **2** showed a blue shift of fluorescence from 470 to 438 nm and **3** fluorescence was blue-shifted from 467 to 444 nm at −196 °C. The blue-shifted fluorescence at −196 °C could be attributed to the freezing of DMF solution that might hinder conversion of coplanar planar LE state to twisted molecular conformation of TICT state. The normal TICT state fluorescence with reduced intensity was observed by increasing the temperature to −6 °C (Figures 2a,b and S10). The intensity was further reduced with a slight blue shifting λ_{max} by increasing to room temperature. In solution, coplanar LE state can easily be converted to twisted TICT state in polar medium. Thus, reversible LE and TICT states at different temperatures lead to reversible fluorescence switching without significant change of intensity.

Table 2. Excited-State Lifetime of 1 and 2

	toluene τ_1 (ns)	$CHCl_3$ τ_1 (ns)	CH_2Cl_2 τ_1 (ns)	CH_3CN τ_1 (ns)	CH_3OH τ_1 (ns)	DMF τ_1 (ns)
1	2.15	3.11	3.60	4.75	3.38	4.60
2	1.67	2.45	2.84	3.86	3.62	3.71

It is noted that the fluorescence λ_{max} at −196 °C in DMF as well as in toluene solution is nearly the same for **1** and **3**. The blue-shifted LE state fluorescence at −196 °C has also been observed in other polar solvents such as CH_3CN, CH_3OH, and ethanol (Figure S12); however, DMF was chosen to investigate heat-dependent fluorescence switching in view of its higher boiling point. TICT formation in DMF prompted to explore rare TICT-induced fluorescence enhancement with

DOI: 10.1021/acsomega.8b03099
ACS Omega 2019, 4, 5147−5154

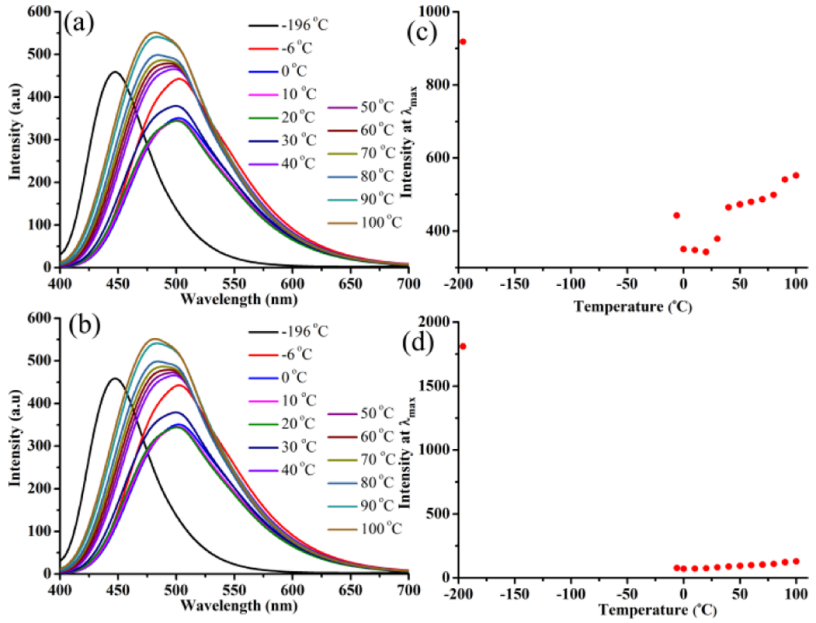

Figure 2. Temperature-dependent fluorescence spectra and variation of intensity at λ_{max} of (a,c) **1** and (b,d) **2** in DMF (10^{-5} M). The intensity of peak at −196 °C has been divided by a factor of (a) 2 and (b) 15.

increasing temperature.[52,53] Both **1** and **2** did not show significant change in the intensity and λ_{max} between 10 and 30 °C. However, further increase of temperature exhibited gradual enhancement of fluorescence intensity with a blue shift of λ_{max} [501−480 nm (**1**), 475−460 nm (**2**)]. Upon cooling to room temperature, the fluorescence reverts to 501 nm for **1** and 470 nm for **2**. Heating- and cooling-induced reversible fluorescence switching was observed for several cycles without significant change of intensity or peak position. Both **1** and **2** exhibited similar fluorescence in the forward and reverse direction at 30 °C (Figure S13). Excitation spectra of **1**, **2**, and **3** at different temperatures also showed a clear change of peak position (Figure S14). At −196 °C temperature, the TICT band around 400 nm for all three compounds completely disappeared. The peak position has been slightly blue-shifted at 100 °C compared to room temperature (Figure S14a,b). The weak peaks at −196 °C might be due to aggregation of molecules at freezing temperature. In contrast, **3** that showed reduction of fluorescence intensity with increasing temperature showed a red shift of peak position (Figure S14c). The enhancement of fluorescence intensity with temperature could be attributed to the activation of more vibration bands that leads to stronger TICT fluorescence.[32,33] The TICT state often shows weak red-shifted fluorescence because fluorescence from the zero vibrational level of TICT is forbidden.[11] Nevertheless, higher asymmetric vibrational bands of TICT could be used to produce radiative transition from the TICT to ground state. Upon heating, these vibrational bands become activated that increased fluorescence intensity. **3** showed a slight decrease of fluorescence intensity and λ_{max} with increase of temperature (Figure S11). This could be due to the labile acidic proton of hydroxyl group that might form strong intermolecular H-bonding with polar DMF solvent molecules. Thus, **1** and **2** in DMF at room temperature exhibited TICT-induced red-shifted fluorescence, whereas they showed strong enhancement of fluorescence with a blue shift of λ_{max} at −196 °C because of prevention of excited state conformation, and stabilizing LE state and heating of DMF solution lead to TICT-active enhancement of fluorescence intensity with a slight blue shift.

1, **2**, and **3** compounds also showed weak-to-moderate fluorescence in the solid state (Figure 3). **1** and **2** showed

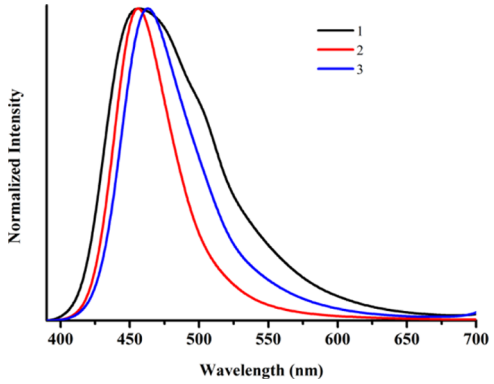

Figure 3. Solid-state fluorescence spectra (λ_{exc} = 360 nm).

fluorescence at 455 nm, whereas **3** showed fluorescence at 463 nm. **1** exhibited relatively weak fluorescence (2.16%) efficiency compared to **2** (10.91%) and **3** (9.45%). Excited-state lifetime studies of all three compounds showed triexponential decay with a similar lifetime (Table S1, Figure S15). At −196 °C, solid-state fluorescence of all three compounds showed slightly blue-shifted fluorescence (Figure S16). This may be due to the reduction of thermal vibration of molecules under low temperature. The fluorescence of **1** and **2** blue-shifted from 455 to 442 nm, whereas the fluorescence of **3** blue-shifted from 464 to 446 nm. The solid-state fluorescence and presence of acid-responsive amine nitrogen is expected to display halochromism.[34] Trifluoroacetic acid (TFA) exposure onto **1** leads to a strong red shift of fluorescence from 455 to 563 nm, whereas NH_3 exposure reverts to initial state (Figure 4a). Similarly, **2** exhibited fluorescence switching between 455 and 587 nm upon TFA exposure followed by NH_3 exposure (Figure 4b). Although TFA exposure of **3** resulted in a strong

DOI: 10.1021/acsomega.8b03099
ACS Omega 2019, 4, 5147−5154

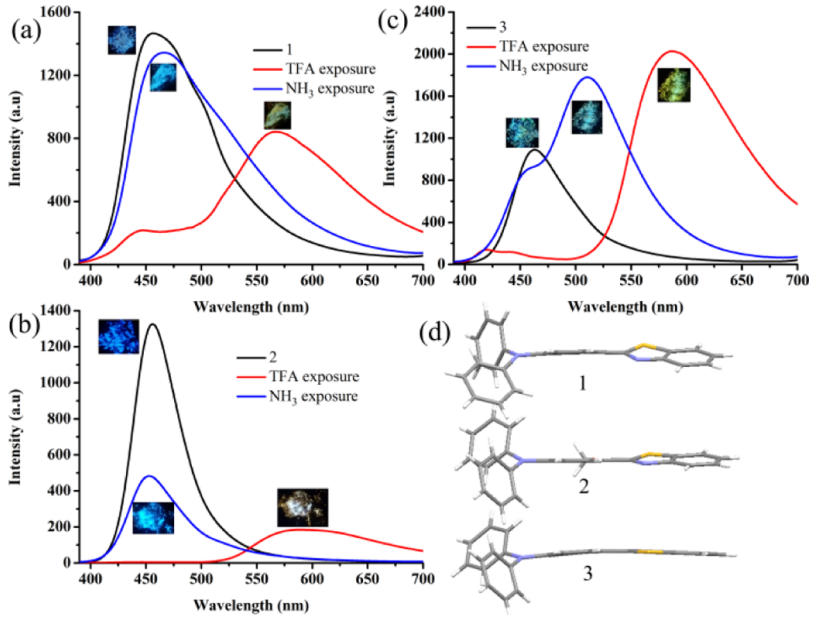

Figure 4. Halochromism of (a) **1**, (b) **2**, and (c) **3** (λ_{exc} 360 nm). (d) Molecular structure of **1**, **2**, and **3** in the crystal lattice. C (gray), N (blue), S (yellow), and H (white).

red shift of fluorescence from 463 to 600 nm, NH_3 exposure did not completely revert the fluorescence to the initial state, rather it blue-shifted to 508 nm with a small hump at 463 nm (Figure 4c). Single-crystal structural analysis for all three compounds has been performed to gain insights into the solid-state fluorescence properties. The TPA group of **1**, **2**, and **3** exhibited a propeller-shaped structure and D−A part of TPA phenyl and imidazole unit exhibited nearly coplanar conformation (Figure 4d). It is noted that the TPA phenyl and imidazole units are slightly twisted in **1** and **2**, whereas perfect planar conformation in **3**. The molecules formed dimer with opposite molecular orientation in the crystal lattice of **1**, **2**, and **3** via weak intermolecular interaction (Figure 5). Twisted molecular conformation of **1** and **2** leads to weak C−H···π intermolecular interactions between molecules in the crystal lattice, whereas planar phenyl and thiazole unit produced strong $\pi\cdots\pi$ interactions in the crystal lattice. The structure collected at room temperature (298 K) as well as at low temperature (100 K) did not show significant variation in the molecular packing (Figures S17−S19). The coplanar conformation along with dimer formation with opposite molecular arrangement produced blue fluorescence in the solid state. To understand the TFA-induced fluorescence switching, we have tried to grow single crystals in the presence of TFA. However, only **3** with TFA produced quality crystals that showed inclusion of two TFA molecules in the crystal lattice (Figure 6). One of the TFA exhibited deprotonation that leads to protonation of benzothiazole nitrogen. The protonation of nitrogen might further increase the electron-withdrawing ability of thiazole and hence leads to red-shifted fluorescence. Strong intermolecular H-bonding between **3** and protonated as well as deprotonated TFA produced dimer in the crystal lattice. Calculation of optical band gap using a single-crystal structure suggested lowest band gap for **3** and highest for **2**, which supported the solid-state fluorescence (Table S1). Highest occupied molecular orbital (HOMO) and lowest unoccupied molecular orbital (LUMO) of **1**, **2**, and **3** has been calculated using Gaussian 09 program package to demonstrate

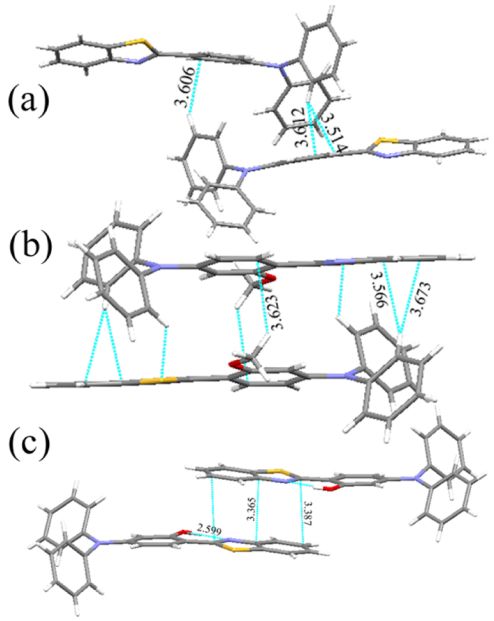

Figure 5. (a) Weak intermolecular interactions induced dimer formation in the crystal lattice of (b) **1**, (b) **2**, and (c) **3**. C (gray), N (blue), S (yellow), and H (white). H-bonds and other interactions (broken line). $d_{D\cdots A}$ distances are marked (Å).

CT from TPA donor to thiazole acceptor (Figure 7). The HOMO of **1**, **2**, and **3** revealed the presence of more electron density on the TPA unit, whereas the electron density was completely transferred to thiazole unit in LUMO.

3. CONCLUSIONS

In conclusion, the fluorescence of TPA−benzothiazole-based D−A derivatives has been modulated by controlling LE and TICT formation in polar solvents, and rare positive enhancement of fluorescence via TICT-active state has also been demonstrated. Solvent-dependent LE and TICT state formation was confirmed using absorption and fluorescence

DOI: 10.1021/acsomega.8b03099
ACS Omega 2019, 4, 5147−5154

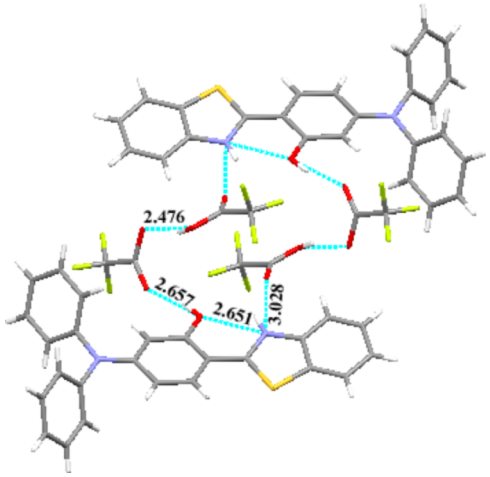

Figure 6. H-bonding interactions between **3** and TFA molecules in the crystal lattice. C (gray), N (blue), S (yellow), and H (white). H-bonding (broken line). $d_{D\cdots A}$ distances are marked (Å).

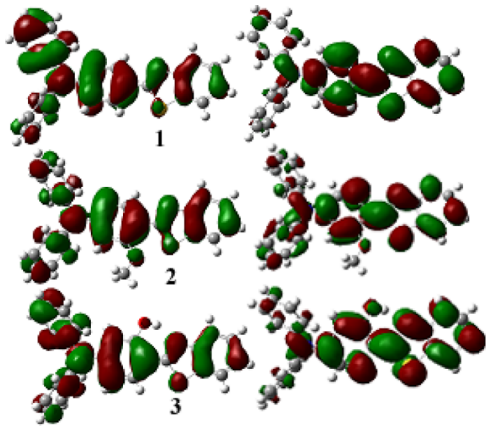

Figure 7. HOMO and LUMO of **1**, **2**, and **3**.

spectra, excited-state lifetime, and quantum yields. Freezing DMF solution of **1**, **2**, and **3** stabilizes the LE state and prevents ultrafast conversion to TICT and exhibits strong enhanced blue-shifted fluorescence. Free mobility of molecules in liquid state undergoes LE to TICT state conversion and shows red-shifted fluorescence. Interestingly, activation of more vibrational bands of TICT state upon heating the DMF solution leads to increase of fluorescence intensity with a slight blue shift of fluorescence. Solid-state structural analysis revealed more planar D−A conformation and dimer formation in the crystal lattice that exhibited blue fluorescence. The acid-responsive imidazole nitrogen was used for demonstrating halochromism. Thus, the fluorescence properties of D−A molecules could be switched reversibly by controlling the temperature.

4. EXPERIMENTAL SECTION

DMF (high-performance liquid chromatography grade), $POCl_3$, TPA, 3-methoxy TPA, and BBr_3 were purchased from Sigma-Aldrich and used without further purification. 2-Aminobenzenethiol was purchased from Alfa Aesar. Solvents were obtained from Merck India. Aldehyde-functionalized TPA molecules were synthesized by following the reported procedure.[48]

4.1. General Synthetic Procedure (Scheme S1).

Benzothiazole-attached TPA D−A derivatives (**1**−**3**) were synthesized by following the reported procedure.[41,42] Typically, TPA aldehyde (1.0 mmol) and 2-aminobenzenethiol (1.0 mmol) were refluxed in dimethyl sulfoxide (1 mL) for 2 h. After cooling, the reaction mixture was dumped into cold water that produced a precipitate. The precipitate was filtered and dried under vacuum. Finally, the compounds were purified using column chromatography.

*4.1.1. N-(4-(Benzo[d]thiazol-2-yl)phenyl)-N-phenyl-benzenamine (**1**).* mp 142−144 °C. Yield = 98%. ^{1}H NMR (300 MHz, $CDCl_3$): δ 8.03 (d, J = 7.8 Hz, 1H), 7.92 (d, J = 9.0 Hz, 2H), 7.87 (d, J = 7.8 Hz, 1H), 7.47 (dt, J = 1.1, 7.8 Hz, 1H), 7.37 (d, J = 1.2 Hz, 1H), 7.35−7.29 (m, 4H), 7.18−7.14 (m, 4H), 7.11−7.09 (m, 4H). ^{13}C NMR (75 MHz, $CDCl_3$): δ 167.9, 154.1, 150.5, 146.9, 134.7, 129.5, 129.2, 128.6, 126.4, 126.3, 125.5, 124.8, 124.1, 122.7, 121.7, 121.5. m/z calcd for $C_{25}H_{18}N_2S$ (M + H): 378.1; found, 378.1.

*4.1.2. N-(4-(Benzo[d]thiazol-2-yl)-3-methoxyphenyl)-N-phenylbenzenamine (**2**).* mp 157−159 °C. Yield = 97%. ^{1}H NMR (300 MHz, $CDCl_3$): δ 8.34 (d, J = 8.7 Hz, 1H), 8.03 (d, J = 8.1 Hz, 1H), 7.89 (d, J = 8.1 Hz, 1H), 7.46 (dt, J = 1.2, 7.6 Hz, 1H), 7.35−7.29 (m, 5H), 7.19−7.17 (m, 4H), 7.14−7.09 (m, 2H), 6.74 (dd, J = 8.7 Hz, 1H), 6.66 (d, J = 2.1 Hz, 1H), 3.85 (s, 3H). ^{13}C NMR (75 MHz, $CDCl_3$): δ 163.3, 158.2, 152.1, 151.4, 146.8, 135.6, 130.2, 129.5, 129.1, 125.8, 125.6, 124.2, 124.1, 122.2, 121.1, 115.6, 114.7, 104.5, 55.6. m/z calcd for $C_{26}H_{20}N_2OS$ (M + H): 408.1; found, 408.1.

*4.1.3. 2-(Benzo[d]thiazol-2-yl)-5-(diphenylamino)phenol (**3**).* mp 164−166 °C. Yield = 95%. ^{1}H NMR (300 MHz, $CDCl_3$): δ 7.92 (d, J = 7.8 Hz, 1H), 7.84 (d, J = 8.1 Hz, 1H), 7.49−7.44 (m, 2H), 7.38−7.29 (m, 5H), 7.19−7.10 (m, 6H), 6.64 (d, J = 2.1 Hz, 1H), 6.56 (dd, J = 8.7, 6.6 Hz, 1H). ^{13}C NMR (75 MHz, $CDCl_3$): δ 169.1, 159.2, 152.0, 151.9, 146.5, 132.2, 129.5, 129.1, 126.5, 126.1, 124.9, 124.5, 121.6, 121.4, 112.6, 110.3, 108.1. m/z calcd for $C_{26}H_{20}N_2OS$ (M + H): 394.1; found, 394.2.

4.2. Characterization.

Nuclear magnetic resonance (NMR) spectra were measured on a Bruker 300 MHz AVANCE-II. Absorption spectra were recorded using PerkinElmer 1050. Fluorescence spectra and absolute quantum yield for all compounds in the solid state were recorded using JASCO fluorescence spectrometer-FP-8300 instruments equipped with integrating sphere and calibrated light source. Lifetime measurements were carried out with a Hamamatsu Photonics Quantaurus-Tau. Mass spectra were recorded with a Bruker 320-MS triple quadrupole mass spectrometer using the direct probe insertion method. Single crystals were coated with paratone-N oil, and the diffraction data were measured at 100 K with synchrotron radiation (λ = 0.62998 Å) on an ADSC Quantum-210 detector at 2D SMC with a silicon (111) double-crystal monochromator at the Pohang Accelerator Laboratory, Korea. CCDC nos.—1858884−1858886 and 1875665 contain the supplementary crystallographic data for this paper. The HOMO, LUMO, and band gap of all structures are studied using B3PW91/6-31+G(d,p) level theory (Gaussian 09 package). The calculations have been performed using TD-DFT-B3PW91 method with 6-31+G(d,p) basis set at the $CHCl_3$ solvent medium using Gaussian 09 program package.

DOI: 10.1021/acsomega.8b03099
ACS Omega 2019, 4, 5147−5154

■ ASSOCIATED CONTENT

Supporting Information

The Supporting Information is available free of charge on the ACS Publications website at DOI: 10.1021/acsomega.8b03099.

Synthesis scheme, NMR spectra, crystallographic table, fluorescence spectra, crystal structure, HOMO−LUMO molecular diagram, lifetime, differential scanning calorimetry and powder X-ray diffraction studies (PDF)

■ AUTHOR INFORMATION

Corresponding Authors

*E-mail: dmoon@postech.ac.kr. Phone: +914362264101. Fax: +914362264120 (D.M.).

*E-mail: philip@biotech.sastra.edu (S.P.A.).

ORCID

Yoshimitsu Sagara: 0000-0003-2502-3041

Dohyun Moon: 0000-0002-6903-0270

Savarimuthu Philip Anthony: 0000-0002-9023-0920

Notes

The authors declare no competing financial interest.

■ ACKNOWLEDGMENTS

The financial support from the Science and Engineering Research Board (SERB), New Delhi, India (SERB no. EMR/2015/00-1891), is acknowledged with gratitude. The CRF facility of SASTRA Deemed University is also acknowledged for absorption spectroscopy. "X-ray crystallography" at the PLS-II 2D-SMC beamline was supported in part by MSIP and POSTECH. The Basic Science Research Program through the National Research Foundation of Korea (NRF) was funded by the Ministry of Education, Science and Technology (NRF-2017R1C1B2003111) for recording mass spectra.

■ REFERENCES

(1) Thomas, S. W.; Joly, G. D.; Swager, T. M. Chemical Sensors Based on Amplifying Fluorescent Conjugated Polymers. *Chem. Rev.* **2007**, *107*, 1339−1386.

(2) Liu, B.; Li, X.-L.; Tao, H.; Zou, J.; Xu, M.; Wang, L.; Peng, J.; Cao, Y. Manipulation of exciton distribution for high-performance fluorescent/phosphorescent hybrid white organic light-emitting diodes. *J. Mater. Chem. C* **2017**, *5*, 7668.

(3) Grimsdale, A. C.; Leok Chan, K.; Martin, R. E.; Jokisz, P. G.; Holmes, A. B. Synthesis of Light-Emitting Conjugated Polymers for Applications in Electroluminescent Devices. *Chem. Rev.* **2009**, *109*, 897−1091.

(4) Wong, M. Y.; Zysman-Colman, E. Purely Organic Thermally Activated Delayed Fluorescence Materials for Organic Light-Emitting Diodes. *Adv. Mater.* **2017**, *29*, 1605444.

(5) Peckus, D.; Matulaitis, T.; Franckevičius, M.; Mimaitė, V.; Tamulevičius, T.; Simokaitienė, J.; Volyniuk, D.; Gulbinas, V.; Tamulevičius, S.; Gražulevičius, J. V. Twisted Intramolecular Charge Transfer States in Trinary Star-Shaped Triphenylamine-Based Compounds. *J. Phys. Chem. A* **2018**, *122*, 3218−3226.

(6) Shimizu, M.; Hiyama, T. Organic Fluorophores Exhibiting Highly Efficient Photoluminescence in the Solid State. *Chem.—Asian J.* **2010**, *5*, 1516−1531.

(7) Anthony, S. P. Organic Solid-State Fluorescence: Strategies for Generating Switchable and Tunable Fluorescent Materials. *ChemPlusChem* **2012**, *77*, 518−531.

(8) He, Z.; Zhang, L.; Mei, J.; Zhang, T.; Lam, J. W. Y.; Shuai, Z.; Dong, Y. Q.; Tang, B. Z. Polymorphism-Dependent and Switchable Emission of Butterfly-Like Bis(diarylmethylene)dihydroanthracenes. *Chem. Mater.* **2015**, *27*, 6601−6607.

(9) Xu, B.; He, J.; Mu, Y.; Zhu, Q.; Wu, S.; Wang, Y.; Zhang, Y.; Jin, C.; Lo, C.; Chi, Z.; Lien, A.; Liu, S.; Xu, J. Very Bright Mechanoluminescence and Remarkable Mechanochromism Using a Tetraphenylethene Derivative with Aggregation-Induced Emission. *Chem. Sci.* **2015**, *6*, 3236−3241.

(10) Zhang, G.; Lu, J.; Sabat, M.; Fraser, C. L. Polymorphism and Reversible Mechanochromic Luminescence for Solid-State Difluoroboron Avobenzone. *J. Am. Chem. Soc.* **2010**, *132*, 2160−2162.

(11) Grabowski, Z. R.; Rotkiewicz, K.; Rettig, W. Structural Changes Accompanying Intramolecular Electron Transfer: Focus on Twisted Intramolecular Charge-Transfer States and Structures. *Chem. Rev.* **2003**, *103*, 3899−4032.

(12) Sasaki, S.; Drummen, G. P. C.; Konishi, G.-I. Recent advances in twisted intramolecular charge transfer (TICT) fluorescence and related phenomena in materials chemistry. *J. Mater. Chem. C* **2016**, *4*, 2731−2743.

(13) Sasaki, S.; Niko, Y.; Igawa, K.; Konishi, G.-I. Aggregation-induced emission active D-π-A binaphthyl luminophore with dual-mode fluorescence. *RSC Adv.* **2014**, *4*, 33474−33477.

(14) Sasaki, S.; Hattori, K.; Igawa, K.; Konishi, G.-i. Directional Control of π-Conjugation Enabled by Distortion of the Donor Plane in Diarylaminoanthracenes: A Photophysical Study. *J. Phys. Chem. A* **2015**, *119*, 4898−4906.

(15) Zhu, L.; Zhao, Y. Cyanostilbene-based intelligent organic optoelectronic materials. *J. Mater. Chem. C* **2013**, *1*, 1059−1065.

(16) Sunahara, H.; Urano, Y.; Kojima, H.; Nagano, T. Design and Synthesis of a Library of BODIPY-Based Environmental Polarity Sensors Utilizing Photoinduced Electron-Transfer-Controlled Fluorescence ON/OFF Switching. *J. Am. Chem. Soc.* **2007**, *129*, 5597−5604.

(17) Drummen, G. P. C.; van Liebergen, L. C. M.; Op den Kamp, J. A. F.; Post, J. A. C11-BODIPY581/591, an oxidation-sensitive fluorescent lipid peroxidation probe: (micro)spectroscopic characterization and validation of methodology. *Free Radical Biol. Med.* **2002**, *33*, 473−490.

(18) Sumalekshmy, S.; Gopidas, K. R. Photoinduced Intramolecular Charge Transfer in Donor−Acceptor Substituted Tetrahydropyrenes†. *J. Phys. Chem. B* **2004**, *108*, 3705−3712.

(19) Chen, B.; Ding, Y.; Li, X.; Zhu, W.; Hill, J. P.; Ariga, K.; Xie, Y. Steric hindrance-enforced distortion as a general strategy for the design of fluorescence "turn-on" cyanide probes. *Chem. Commun.* **2013**, *49*, 10136−10138.

(20) Suhina, T.; Weber, B.; Carpentier, C. E.; Lorincz, K.; Schall, P.; Bonn, D.; Brouwer, A. M. Fluorescence Microscopy Visualization of Contacts Between Objects. *Angew. Chem., Int. Ed.* **2015**, *54*, 3688−3691.

(21) Shi, J.; Chang, N.; Li, C.; Mei, J.; Deng, C.; Luo, X.; Liu, Z.; Bo, Z.; Dong, Y. Q.; Tang, B. Z. Locking the phenyl rings of tetraphenylethene step by step: understanding the mechanism of aggregation-induced emission. *Chem. Commun.* **2012**, *48*, 10675−10677.

(22) Gong, Y.; Zhang, Y.; Yuan, W. Z.; Sun, J. Z.; Zhang, Y. D-A Solid Emitter with Crowded and Remarkably Twisted Conformations Exhibiting Multifunctionality and Multicolor Mechanochromism. *J. Phys. Chem. C* **2014**, *118*, 10998−11005.

(23) Sasaki, S.; Igawa, K.; Konishi, G.-I. The effect of regioisomerism on the solid-state fluorescence of bis(piperidyl)anthracenes: structurally simple but bright AIE luminogens. *J. Mater. Chem. C* **2015**, *3*, 5940−5950.

(24) Li, W.; Pan, Y.; Yao, L.; Liu, H.; Zhang, S.; Wang, C.; Shen, F.; Lu, P.; Yang, B.; Ma, Y. A Hybridized Local and Charge-Transfer Excited State for Highly Efficient Fluorescent OLEDs: Molecular Design, Spectral Character, and Full Exciton Utilization. *Adv. Opt. Mater.* **2014**, *2*, 892−901.

(25) Uoyama, H.; Goushi, K.; Shizu, K.; Nomura, H.; Adachi, C. Highly efficient organic light-emitting diodes from delayed fluorescence. *Nature* **2012**, *492*, 234−238.

(26) Yuan, W. Z.; Bin, X.; Chen, G.; He, Z.; Liu, J.; Ma, H.; Peng, Q.; Wei, B.; Gong, Y.; Lu, Y.; He, G.; Zhang, Y. Achieving Hybridized

DOI: 10.1021/acsomega.8b03099
ACS Omega 2019, 4, 5147−5154

Local and Charge-Transfer Excited State and Excellent OLED Performance Through Facile Doping. *Adv. Opt. Mater.* **2017**, *5*, 1700466.
(27) Goh, W. L.; Lee, M. Y.; Joseph, T. L.; Quah, S. T.; Brown, C. J.; Verma, C.; Brenner, S.; Ghadessy, F. J.; Teo, Y. N. Molecular Rotors As Conditionally Fluorescent Labels for Rapid Detection of Biomolecular Interactions. *J. Am. Chem. Soc.* **2014**, *136*, 6159−6162.
(28) Cao, K.; Farahi, M.; Dakanali, M.; Chang, W. M.; Sigurdson, C. J.; Theodorakis, E. A.; Yang, J. Aminonaphthalene 2-Cyanoacrylate (ANCA) Probes Fluorescently Discriminate between Amyloid-β and Prion Plaques in Brain. *J. Am. Chem. Soc.* **2012**, *134*, 17338−17341.
(29) Hariharan, P. S.; Venkataramanan, N. S.; Moon, D.; Anthony, S. P. Self-Reversible Mechanochromism and Thermochromism of a Triphenylamine-Based Molecule: Tunable Fluorescence and Nanofabrication Studies. *J. Phys. Chem. C* **2015**, *119*, 9460−9469.
(30) Chandrasekharan, N.; Kelly, L. A. A Dual Fluorescence Temperature Sensor Based on Perylene/Exciplex Interconversion. *J. Am. Chem. Soc.* **2001**, *123*, 9898−9899.
(31) Feng, J.; Tian, K.; Hu, D.; Wang, S.; Li, S.; Zeng, Y.; Li, Y.; Yang, G. A Triarylboron-Based Fluorescent Thermometer: Sensitive Over a Wide Temperature Range. *Angew. Chem., Int. Ed.* **2011**, *50*, 8072−8076.
(32) Cao, C.; Liu, X.; Qiao, Q.; Zhao, M.; Yin, W.; Mao, D.; Zhang, H.; Xu, Z. A Twisted-Intramolecular-Charge-Transfer (TICT) based Ratiometric Fluorescent Thermometer with a Mega-Stokes Shift and a Positive Temperature Coefficient. *Chem. Commun.* **2014**, *50*, 15811−15814.
(33) Chen, X.; Zhang, X.; Zhang, G. Wide-range thermochromic luminescence of organoboronium complexes. *Chem. Commun.* **2015**, *51*, 161−163.
(34) Hariharan, P. S.; Mothi, E. M.; Moon, D.; Anthony, S. P. Halochromic Isoquinoline with Mechanochromic Triphenylamine: Smart Fluorescent Material for Rewritable and Self-Erasable Fluorescent Platform. *ACS Appl. Mater. Interfaces* **2016**, *8*, 33034.
(35) Thomas, K. R. J.; Lin, J. T.; Tao, Y. T.; Ko, C. W. New Star-Shaped Luminescent Triarylamines: Synthesis, Thermal, Photophysical, and Electroluminescent Characteristics. *Chem. Mater.* **2002**, *14*, 1354−1361.
(36) Hariharan, P. S.; Gayathri, P.; Kundu, A.; Karthikeyan, S.; Moon, D.; Anthony, S. P. Synthesis of tunable, red fluorescent aggregation-enhanced emissive organic fluorophores: stimuli-responsive high contrast off-on fluorescence switching. *CrystEngComm* **2018**, *20*, 643−651.
(37) Fu, H.-Y.; Liu, X.-J.; Xia, M. Tunable solid state emission of novel V-shaped fluorophores by subtle structure modification: polymorphism, mechanofluoro-chromism and micro-fabrication. *RSC Adv.* **2017**, *7*, 50720−50728.
(38) Wang, H.-Y.; Chen, G.; Xu, X.-P.; Ji, S.-J. Synthesis and characterization of triphenylamine-benzothiazole-based donor and acceptor materials. *Synth. Met.* **2010**, *160*, 1065−1072.
(39) Hariharan, P. S.; Gayathri, P.; Moon, D.; Anthony, S. P. Tunable and Switchable Solid State Fluorescence: Alkyl Chain Length-Dependent Molecular Conformation and Self-Reversible Thermochromism. *ChemistrySelect* **2017**, *2*, 7799.
(40) Yao, D.; Zhao, S.; Guo, J.; Zhang, Z.; Zhang, H.; Liu, Y.; Wang, Y. Hydroxyphenyl-benzothiazole based full color organic emitting materials generated by facile molecular modification. *J. Mater. Chem.* **2011**, *21*, 3568−3570.
(41) Katariya, S. B.; Patil, D.; Rhyman, L.; Alswaidan, I. A.; Ramasami, P.; Sekar, N. Triphenylamine-based fluorescent NLO phores with ICT characteristics: Solvatochromic and theoretical study. *J. Mol. Struct.* **2017**, *1150*, 493−506.
(42) Yang, Y.; Li, B.; Zhang, L.; Guan, Y. Triphenylamine based benzimidazole and benzothiazole: Synthesis and applications in fluorescent chemosensors and laser dyes. *J. Lumin.* **2014**, *145*, 895−898.
(43) Wang, H.-Y.; Chen, G.; Xu, X.-P.; Ji, S.-J. Synthesis and characterization of triphenylamine-benzothiazole-based donor and acceptor materials. *Synth. Met.* **2010**, *160*, 1065−1072.
(44) Valdebenito, S.; Zanocco, R.; Günther, G.; Lemp, E.; Zanocco, A. L. Solvent and compartmentalization effects on the photophysics of 4-(benzothiazol-2-yl)-N,N-diphenylaniline. *Afinidad* **2011**, *68*, 226−233.
(45) Padalkar, V. S.; Seki, S. Excited-state intramolecular proton-transfer (ESIPT)-inspired solid state emitters. *Chem. Soc. Rev.* **2016**, *45*, 169−202.
(46) Kundu, A.; Karthikeyan, S.; Moon, D.; Anthony, S. P. Self-reversible thermofluorochromism of D-A-D triphenylamine derivatives and the effect of molecular conformation and packing. *CrystEngComm* **2017**, *19*, 6979.
(47) Hariharan, P. S.; Prasad, V. K.; Nandi, S.; Anoop, A.; Moon, D.; Anthony, S. P. Molecular Engineering of Triphenylamine Based Aggregation Enhanced Emissive Fluorophore: Structure-Dependent Mechanochromism and Self-Reversible Fluorescence Switching. *Cryst. Growth Des.* **2017**, *17*, 146.
(48) Sakai, K.-i.; Ishikawa, T.; Akutagawa, T. A blue-white-yellow color-tunable excited state intramolecular proton transfer (ESIPT) fluorophore: sensitivity to polar-nonpolar solvent ratios. *J. Mater. Chem. C* **2013**, *1*, 7866−7871.
(49) Yao, L.; Zhang, S.; Wang, R.; Li, W.; Shen, F.; Yang, B.; Ma, Y. Highly Efficient Near-Infrared Organic Light-Emitting Diode Based on a Butterfly-Shaped Donor-Acceptor Chromophore with Strong Solid-State Fluorescence and a Large Proportion of Radiative Excitons. *Angew. Chem., Int. Ed.* **2014**, *126*, 2151.
(50) Ouyang, X.; Li, X.-L.; Ai, L.; Mi, D.; Ge, Z.; Su, S.-J. Novel "Hot Exciton" Blue Fluorophores for High Performance Fluorescent/Phosphorescent Hybrid White Organic Light-Emitting Diodes with Superhigh Phosphorescent Dopant Concentration and Improved Efficiency Roll-Off. *ACS Appl. Mater. Interfaces* **2015**, *7*, 7869−7877.
(51) Wang, X.-d.; Wolfbeis, O. S.; Meier, R. J. Luminescent Probes and Sensors for Temperature. *Chem. Soc. Rev.* **2013**, *42*, 7834−7869.
(52) Okabe, K.; Inada, N.; Gota, C.; Harada, Y.; Funatsu, T.; Uchiyama, S. Intracellular Temperature Mapping with a Fluorescent Polymeric Thermometer and Fluorescence Lifetime Imaging Microscopy. *Nat. Commun.* **2012**, *3*, 705.
(53) Jiang, Z.; Chen, Y.; Yang, C.; Cao, Y.; Tao, Y.; Qin, J.; Ma, D. A Fully Diarylmethylene-Bridged Triphenylamine Derivative as Novel Host for Highly Efficient Green Phosphorescent OLEDs. *Org. Lett.* **2009**, *11*, 1503−1506.

DOI: 10.1021/acsomega.8b03099
ACS Omega 2019, 4, 5147−5154